Ceramics International 42 (2016) 14754–14759

Contents lists available at ScienceDirect

Ceramics International

journal homepage: www.elsevier.com/locate/ceramint

Electronic structure of transparent conducting Mo-doped indium oxide films grown by polymer assisted solution process

Aeran Song [a], Hyun-Woo Park [a], Sujaya Kumar Vishwanath [b], Jihoon Kim [b], Ju-Yeoul Baek [c], Kyoung-Jun Ahn [c], Kwun-Bum Chung [a,*]

[a] Department of Physics, Dongguk University, Seoul 04620, Republic of Korea
[b] Division of Advanced Materials Engineering, Kongju National University, Cheonan, Chungchungnam-do 32588, Korea
[c] Department of R&D Center, SNTEK Co., Suwon, Gyeonggi-do 16643, Korea

ARTICLE INFO

Article history:
Received 5 April 2016
Received in revised form
6 June 2016
Accepted 16 June 2016
Available online 17 June 2016

Keywords:
Molybdenum doped indium oxide
Electronic structure
Transparent conducting oxide
Chemical bonding states
Conduction band offset

ABSTRACT

Transparent conducting properties of molybdenum doped indium oxide thin films by polymer-assisted solution (PAS) were investigated as a function of Mo doping concentration. Indium oxide films with molybdenum of ~1.5% (MIO) showed lowest electrical resistivity with 7.89×10^{-4} Ω cm, compared to those of indium oxide films with 4.39×10^{-3} Ω cm. The enhancement of the transparent conducting properties by molybdenum doping were explained by the electronic structure in terms of chemical bonding states, band edge states below the conduction band, and band alignment. Molybdenum doping into indium oxide films resulted in the evolution of the conduction band and the change of band alignment.

1. Introduction

Transparent conducting oxides (TCOs) thin films have attracted significant interest in terms of their technological realization capabilities for optical and electrical applications (e.g., smart windows, photovoltaic cells, light emitting diodes, and transparent thin film transistors) [1,2]. The required conditions for TCOs for these industrial applications include low electrical resistivity ($\sim10^{-3}$ Ω cm) and high optical transmittance (>80%) in the visible wavelength region.

Among the various TCO films, In based oxides (including InSnO, InZnO, InZnSnO, InSiO) have been widely studied to apply the transparent electronics due to their high mobility, low resistivity, and high near infrared optical transmittance using different doping elements into In oxide matrix [3–5]. In addition, fabrication of TCO films by solution processes has become viable, as most are compatible with deposition at the ambient of atmosphere and on large scale substrate with higher film density and less void fraction [6].

Among various solution processes, the polymer-assisted solution (PAS) process used in this study possesses a merit because water-soluble polymers (e.g., polyethylenimine, PEI) play a significant role in the incorporation of metal ions or metal complexes in the solution, preventing the metal ions from unwanted chemical reactions. This feature results in the homogeneous distribution of the metal ions in the solution, while also affecting the viscosity of the solution and helping to obtain uniform films of the desired thickness by various coating techniques (e.g., spin coating, inkjet printing, dip coating, and spray coating) [7–9].

The main idea of metal-doped InO seeks to achieve a greater valence difference between the dopant and In ion. Metal doping offers the capability to increase the number of free carriers, in order to attain high mobility and low NIR absorption with low impurity. Many researchers have extensively studied metal doped InO, including with elements such as tin (Sn), gallium (Ga), copper (Cu), zirconium (Zr), and titanium (Ti) [3,4,10,11]. Compared to these dopants, Mo ($[Kr]4d^5 5s^1$) can serve as a more beneficial doping element in the In oxide matrix, because it can donate more than three electrons to the free carriers due to the high valence difference. Previous studies have employed various deposition techniques (e.g., activated reactive evaporation, pulsed laser deposition, radio frequency magnetron sputtering, high density plasma evaporation, chemical vapor deposition, and spray pyrolysis technique) for the preparation of In_2O_3 and molybdenum-doped indium oxide (MIO) thin films [12–16]. The reported results had the electrical resistivity with > ~4×10^{-4} Ω cm and optical transmittance with >80% according to the deposition techniques,

* Corresponding author.
E-mail address: kbchung@dongguk.edu (K.-B. Chung).

http://dx.doi.org/10.1016/j.ceramint.2016.06.103
0272-8842/

respectively. However, most of this research has focused on the electrical and optical properties of the Mo-doped InO films, while neglecting to figure out the effect of Mo doping in In_2O_3 or the origin of the changes in the electrical and optical properties.

In this study, we report on Mo-doped indium oxide thin films using a simple and low-cost solution process. We systematically examine the effects of Mo-doping on the electronic structure in terms of chemical bonding states, band edge states below the conduction band, and band alignment as a function of Mo doping concentration.

2. Experiment

To prepare MIO films by the PAS process, indium(III) nitrate hydrate (10 g; Aldrich) and polyethyleneimine (PEI with Mw=25,000; 10 g; Aldrich) were added to the EDTA-dissolved solution (ethylenediamine tetraacetic acid (EDTA, 10 g; Aldrich) in 40 mL of deionized (DI) water) to form In-PAS. pH of solution was controlled by slowly adding NaOH and HCl. Similarly the Mo-PAS was also formulated with ammonium molybdate tetrahydrate (3 g; Aldrich). Both In-and Mo-PAS were filtered separately through a membrane with molecular weight cut-off of 10,000 to remove uncoordinated cations and anions from the solutions. MIO-PAS was prepared by adding the Mo-PAS to In-PAS at different mixing ratios, ranging from 0 at% to 5.0 at% MIO-PAS was spin-coated onto glass substrates at 2000 rpm. The glass substrates were ultrasonically cleaned by acetone, ethanol, and boiled isopropyl alcohol (IPA) prior to the spin-coating process. The PAS-processed MIO films were depolymerized at a temperature of 500 °C in a tube furnace under the mixing gas environment of H_2 forming gas and oxygen (4:1), leading to the growth of MIO thin films. Additional thermal process by rapid thermal annealing (RTA) was employed to electrically activate dopants in the MIO films under oxygen atmosphere at 700 °C.

We assessed the electrical properties (e.g., the carrier concentration, mobility, and resistivity) of MIO films by using a Hall measurement system with a 0.55-Tesla permanent magnet at room temperature. We investigated the chemical bonding states of MIO by x-ray photoelectron spectroscopy (XPS), using a monochromatic Al Kα source. We measured the features of the conduction band and the band edge state below the conduction band by using x-ray absorption spectroscopy (XAS) at the facility of the 2A beam line in Pohang Accelerator Laboratory (PAL), Korea. We carried out the XAS measurement in total electron yield (TEY) mode by detection of the sample current. We examined the electronic structure of the band gap and band alignments (conduction band offset between the minimum of the conduction band and the Fermi energy, ΔE_{CB}) by spectroscopic ellipsometry (SE) and XPS. We obtained SE spectra with incident angles of 65°, 70°, and 75° at photon energies of 0.75–6.4 eV, using a rotating analyzer system with an auto retarder.

3. Results and discussion

Fig. 1(a) shows the carrier concentration, Hall mobility, and resistivity of MIO films as a function of Mo doping concentration. With Mo doping, the resistivity of the MIO films demonstrated a parabolic tendency with the lowest values of 7. 89×10^{-4} Ω cm for MIO film with ~1.5% Mo doping. The lowest resistivity of the MIO film with ~1.5% Mo doping was attributed to increased carrier concentration and Hall mobility. Compared to the $1.92\times10^{20}/cm^3$ carrier concentration and 7.44 cm^2/V s Hall mobility of the indium oxide films, the MIO film with ~1.5% Mo doping showed a higher carrier concentration of $7.51\times10^{20}/cm^3$ and Hall mobility of 10.6 cm^2/V s. As Mo doping increased above 3% Mo doping, the resistivity was increased, and the carrier concentration and Hall mobility were decreased. Optical transmittance in the visible wavelength region was changed by the effect of Mo doping into indium oxide films, as shown in Fig. 1(b). Even if optical transmittance has the similar tendency regardless of Mo doping concentration, MIO film with ~1.5% Mo doping shows the slightly high transmittance in the wavelength below ~500 nm. In order to

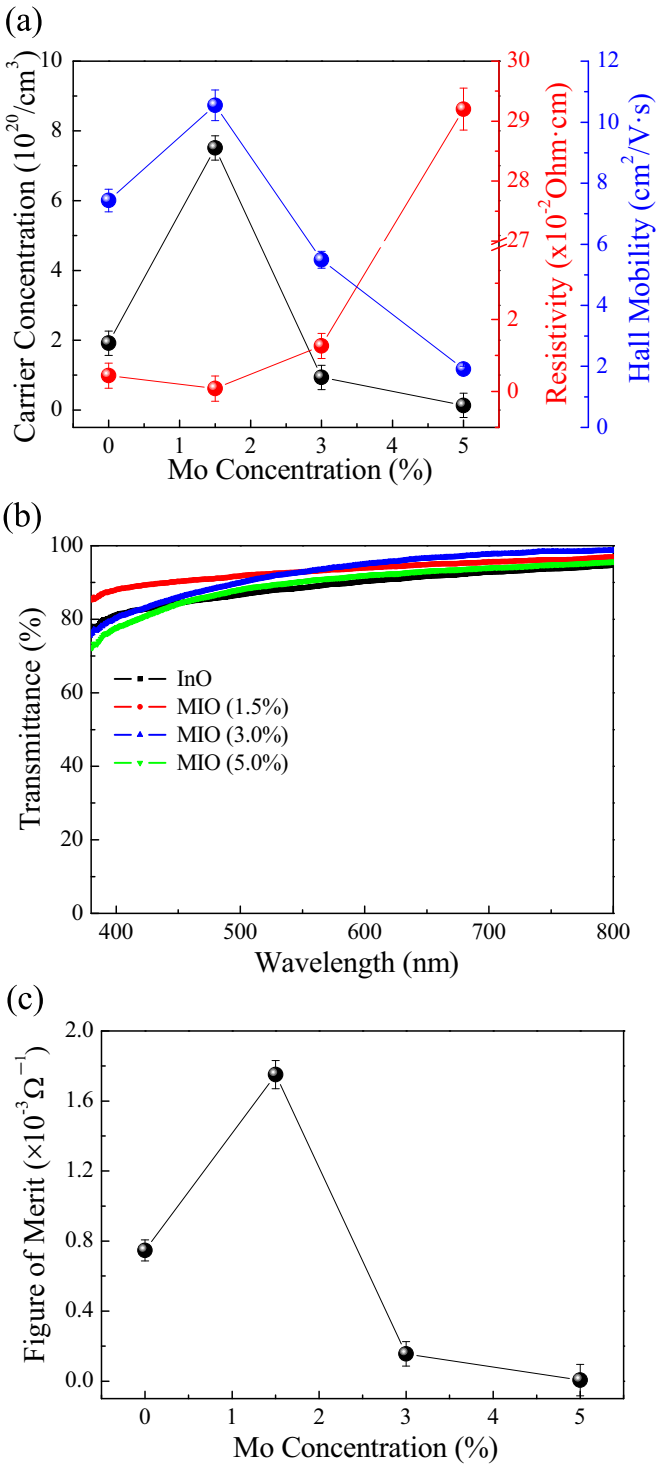

Fig. 1. (a) Electrical properties, including carrier concentration, Hall mobility, and resistivity of MIO films, (b) optical transmittance spectra, and (c) figure of merit (FOM) value as a function of Mo doping concentration.

determine the optimal transparent conducting property of MIO films, we tried to calculate the figure of merit (FOM) using the sheet resistance (R_{sh}) and average optical transmittance (T) between 380 nm and 800 nm. As reported by Haacke, the FOM value calculated using the equation (T^{10}/R_{sh}) represents a useful criterion to determine the optimal conditions of the transparent conducting films, because a higher FOM value represents higher optical transmittance and conductivity [17]. MIO film with ~1.5% Mo doping exhibited the highest FOM value of $1.8 \times 10^{-3}\ \Omega^{-1}$, as shown in Fig. 1(c). The increase of the FOM was caused by the decrease of electrical resistivity depending on the Mo doping concentration.

Fig. 2 shows the core level spectra of In 3*d*, O 1*s*, and Mo 3*d* as a function of Mo doping concentration. We obtained XPS spectra after sputtering by Ne, in order to minimize the surface contamination of the adsorbed OH, C, H_2O, and others. The binding energies of In $3d_{5/2}$ and In $3d_{3/2}$ at 445.4 and 453.0 eV, respectively, in Fig. 2(a) correspond to the binding energy of the In^{3+} in the indium oxide films, being nearly the same between indium oxide and MIO films regardless of Mo doping. However, O 1*s* spectra in Fig. 2(b) were slightly changed by Mo doping into indium oxide films. In order to examine the chemical bonding states of O 1*s*, we carefully deconvoluted the XPS spectra with three different Gaussian peaks (indexed as O1, O2, and O3) from a lower binding

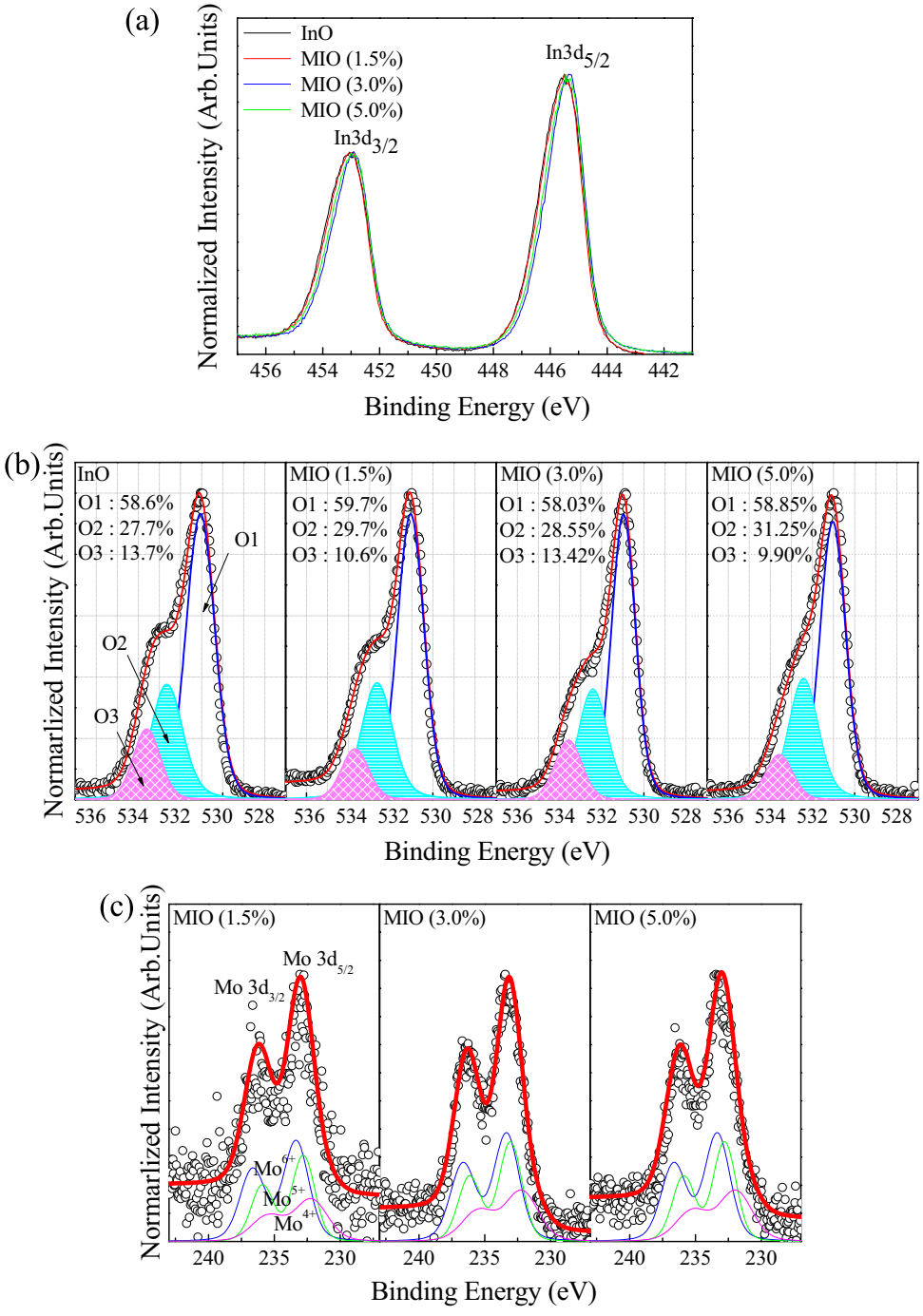

Fig. 2. XPS spectra of indium oxide films for (a) In 3*d*, (b) O 1*s*, and (c) Mo 3*d* of MIO films as a function of Mo doping concentration. O 1*s* and Mo 3*d* in (b) and (c) were deconvoluted with sub-chemical bonding states.

energy. The low binding energy peak (O1) at ~531.1 eV was related to the O_2 ions on the metal oxides, indicating In–O and In–Mo–O bonds. The higher binding energy peak (O3) around 533.7 eV was usually attributed to chemisorbed or dissociated O_2 or OH species on the surface of the oxide films (e.g., $–CO_3$, adsorbed H_2O, or adsorbed O_2). The peak at the medium binding energy (O2) of the O 1s spectrum was associated with OH bonding species and with O^{2-} ions in the oxygen-deficient In–O and In–Mo–O bonding matrix which could be related to the oxygen vacancies. Even though the relative area of the oxygen deficient peak (O2) was slightly increased by Mo doping into indium oxide films, the ratio of the O2 peak among total oxygen composition (O2/O total) had the similar value within the detection limit of XPS, except the increase in MIO film with ~5% Mo doping. The core level spectra of Mo 3*d* based on the Gaussian fits of Mo 3*d* by considering the spectral resolution and spin-orbit splitting, were comprised of Mo^{6+}, Mo^{5+}, and Mo^{4+}. As Mo doping increased, the chemical bonding state of Mo^{6+}, Mo^{5+}, and Mo^{4+} were slightly increased. Previous studies have reported that the chemical bonding states of Mo in the MIO films mainly exists as Mo^{6+} [18]. The sub-oxidation states of Mo^{5+} and Mo^{4+}, as MoO_{3-x} in the In–Mo–O matrix, could create the adjacent oxygen vacancies. Therefore, as based on the changes in chemical bonding states of O 1*s* and Mo 3*d*, those are contrary to the change of carrier concentration and it is difficult to explain the change of electrical properties by Mo doping into indium oxide films. In order to interpret the detailed origin of change in conducting properties by Mo doping, more discussion is provided below and considers the electronic structure including the band edge states below the conduction band and the band alignment.

The detailed electronic structure for the unoccupied states of the conduction band by Mo doping into indium oxide films was obtained by XAS measurement. Fig. 3(a) shows the normalized O K edge spectra of indium oxide and MIO films. We carefully performed normalizations of XAS spectra by subtracting an x-ray beam background, then subsequently scaling pre- and post-edge levels that could be used to compare the qualitative changes of the conduction band [19]. The normalized O K edge spectra of the indium oxide film were directly related to the oxygen p-projected states of the conduction band, consisting of unoccupied hybridization orbitals for In 5*sp*+O 2*p* [20]. The absorption spectra of the MoO_{3-x} incorporated into the In–O matrix were comprised of Mo 4*d*, 5*sp*+ O 2*p* [21]. The conduction band of the MIO film represents In and Mo hybridized orbital peaks, depending on the energy position of the O K edges for indium oxide and MoO_{3-x}; In 5s, Mo 4*d*+O 2*p* (peaks A); and In5*sp*, Mo 5*sp*+O 2*p* (peaks B). Based on the theoretical background, O K edge spectra could be deconvoluted into Gaussian peaks, as shown in Fig. 3(a). Interestingly, the peak (peak A) related to In 5*s*, Mo 4*d*+O 2*p* around ~535 eV was increased by Mo doping into indium oxide up to ~3% Mo doping. Changes of the conduction band could induce the expansion of unoccupied states, thereby improving the charge transport and resulting in lower resistivity [22]. Fig. 3(b) shows a narrow energy region below the conduction band edge, which identifies two distinct band edge states located at the shallow level (D1) and deep level (D2) from the conduction band edge. The

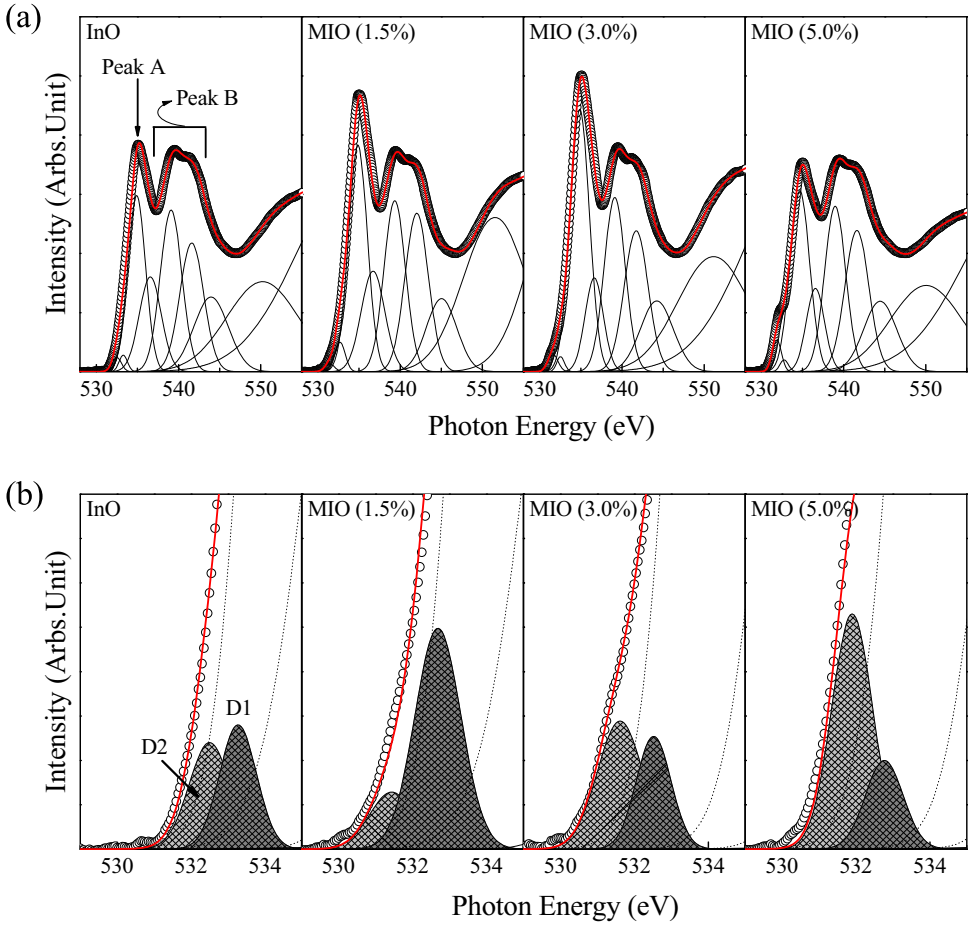

Fig. 3. (a) Normalized XAS O K edge spectra, and Gaussian fits of normalized XAS O K edge spectra, and (b) band edge states below the conduction band, as a function of Mo doping concentration.

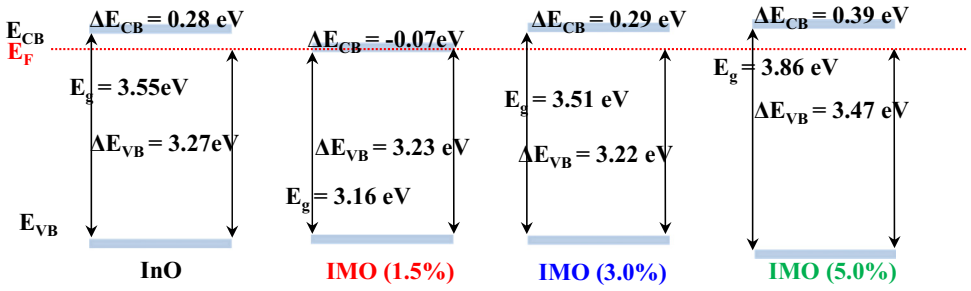

Fig. 4. Schematic energy level diagram, reflecting the relative energy position of the Fermi level (E_F) with respect to the conduction band (E_{CB}) minimum and valence band (E_{VB}) maximum, as a function of Mo doping concentration.

quantitative analysis of unoccupied states by D1 and D2 has similar amount up to ~3% Mo doping. MIO film with ~5% Mo doping shows the larger band edge state in the deep level (D2) from the conduction band edge due to the increase of incorporation of unoccupied states by MoO_{3-x}. However, the relative ratio between shallow band edge state (D1) and deep band edge state (D2) has the complex tendencies as a function of Mo doping concentration, which represent that MIO film with ~1.5% Mo doping (with highest carrier concentration and Hall mobility) has higher D1 state and lower D2 state, and MIO film with ~5% Mo doping (with lowest carrier concentration and Hall mobility) has lower D1 state and higher D2 state. In a previous study, a correlation with the electrical properties of the ZnO film, such as carrier concentration and mobility, has been related to the relative energy level and qualitative change [23]. The most plausible interpretation for the changes in electrical properties such as carrier concentration and mobility can be attributed to the evolution of the band edge states as a function of Mo doping concentration. The change of the carrier concentration as a function of Mo doping concentration, may be explained by the increase of the shallow band edge state (D1) because it means that the number of free electron which can conduct as a carrier is increasing with the generation of oxygen vacancies, and it is close to the conduction band edge [24]. The Hall mobility is associated with the deep band edge state (D2), which can have a higher effect on the degradation of the mobility by the unoccupied states because of charge trapping and an increase in charge scattering during carrier transport due to energy levels being far from the conduction band.

Fig. 4 shows the schematic energy diagram of valence band maximum, conduction band minimum, and Fermi level as a function of Mo doping concentration. Considering the band gap (by SE) and the valence band offset (by XPS) between the Fermi level and the valence band maximum, we could obtain the schematic energy diagram for the conduction band offset (the energy difference between the minimum of the conduction band and the Fermi energy, ΔE_{CB}), as shown in Fig. 4. The conduction band offset decreased by Mo doping into indium oxide up to ~1.5% Mo doping and increased above ~1.5% Mo doping. These are related to the changes of carrier concentration by the enhancement of the probability of electron transfer from occupied states to unoccupied states in the conduction band, similar to the evolution of shallow band edge state (D1) in Fig. 3(b) [25].

4. Conclusions

We grew molybdenum-doped indium oxide (MIO) films on glass substrates using a polymer assisted solution process. We investigated the transparent conducting properties of the MIO films as a function of Mo doping concentration. ~1.5% Mo doping into the indium oxide films induced lowest electrical resistivity of 7.89×10^{-4} Ω cm, compared to indium oxide and higher Mo-doped indium oxide films. Changes in electrical properties of MIO films is related to the evolution of the electronic structure depending on Mo doping concentration. The unoccupied states in the shallow level and in the deep level from the conduction band, were related to the change of carrier concentration and Hall mobility, respectively. In addition, ~1.5% Mo-doped indium oxide films with highest carrier concentration represented the smallest conduction band offset (ΔE_{CB}).

Acknowledgement

This research was supported by the “Sensitivity touch platform development and new industrialization support program” through the Ministry of Trade, Industry & Energy and the Korea Institute for Advancement of Technology (R0002657) and Basic Science Research Program through the National Research Foundation of Korea (NRF) funded by the Ministry of Education, Science and Technology (2016R1A6A1A03012877).

References

[1] Tadatsugu Minami, Semicond. Sci. Tech. 20 (2005) S35.
[2] Elvira Fortunato, David Ginley, Hideo Hosono, David C. Paine, MRS Bull. 32 (2007) 242.
[3] H. Kim, C.M. Gilmore, A. Piqué, J.S. Horwitz, H. Mattoussi, H. Murata, Z.H. Kafafi, D. B. Chrisey, J. Appl. Phys. 86 (1999) 6451.
[4] N. Ito, Y. Sato, P.K. Song, A. Kaijio, K. Inoue, Y. Shigesato, Thin Solid Films 496 (2006) 99.
[5] Hye.-Min. Lee, Sin.-Bi. Kang, Kwun.-Bum. Chung, Han.-Ki. Kim, Appl. Phys. Lett. 102 (2013) 021914.
[6] Jin.-Suk. Seo, Jun.-Hyuck. Jeon, Young Hwan Hwang, Hyungjin Park, Minki Ryu, Sang.-Hee. Park, Byeong.-Soo. Bae, Sci. Rep. 3 (2013) 2085.
[7] Q.X. Jia, T.M. Mccleskey, A.K. Burrell, Y. Lin, G.E. Collis, H. Wang, A.D.Q. Li, S. R. Folytyn, Nat. Mater. 3 (2004) 529.
[8] G.F. Zou, J. Zhao, H.M. Luo, T.M. McCleskey, A.K. Burrell, Q.X. Jia, Chem. Soc. Rev. 42 (2013) 439.
[9] S.K. Vishwanath, W. Jin, J. Kang, J. Kim, J. Alloy. Compd. 631 (2015) 67.
[10] Caroline E. Knapp, Geoffrey Hyett, Ivan P. Parkin, Claire J. Carmalt, Chem. Mat. 23 (2011) 1719.
[11] Timo Asikainen, Mikko Ritala, Markku Leskela, Thin Solid Films 440 (2003) 152.
[12] S. Kaleemulla, N. Madhusudhana Rao, M. Girish Joshi, A. Sivasankar Reddy, S. Uthanna, P. Sreedhara Reddy, J. Alloy. Compd. 504 (2010) 351.
[13] D. Beena, R. Vinodkumar, I. Navas, V. Ganesan, A. Yamuna, V.P. Mahadevan Pillai, J. Alloy. Compd. 539 (2012) 63.
[14] Elangovan Elamurugu, Parthiban Shanmugam, Gonçalo Gonçalves, Nuno Franco, Eduardo Alves, Rodrigo Martins, Elvira Fortunato, EPL 97 (2012) 36002.
[15] Davinder S. Bhachu, David O. Scanlon, Gopinathan Sankar, T.D. Veal, Russell G. Egdell, Giannantonio Cibin, Andrew J. Dent, Caroline E. Knapp, Claire J. Carmalt, Ivan P. Parkin, Chem. Mater. 27 (2015) 2788.
[16] S. Parthiban, E. Elangovan, K. Ramamurthi, R. Martins, E. Fortunato, Sol. Energy Mater. Sol. Cells 94 (2010) 406.
[17] G. Haacke, J. Appl. Phys. 47 (1976) 4086.
[18] Yang Meng, Xi.-liang. Yang, Hua.-xian. Chen, Jie Shen, Yi.-ming. Jiang, Zhuang.-jian. Zhang, Zhong.-yi. Hua, Thin Solid Films 394 (2001) 218.
[19] K.B. Chung, J.P. Long, H. Seo, G. Lucovsky, D. Nordlund, J. Appl. Phys. 106 (2009) 074102.
[20] H.-M. Lee, S.-B. Kang, K.-B. Chung, H.-K. Kim, Appl. Phys. Lett. 102 (2013) 021914.

[21] Lingyun Liu, Wenhua Zhang, Panpan Guo, a Kai Wang, Jiaou Wang, Haijie Qian, Ibrahim Kurash, Chia.-Hsin. Wang, Yaw.-Wen. Yang, Faqiang Xu, Phys. Chem. Chem. Phys. 17 (2015) 3463.
[22] Hye.-Min. Lee, Yong.-Jin. Noh, Seok.-In. Na, Kwun.-Bum. Chung, Han.-Ki. Kim, Sol. Energy Mater. Sol. Cells 125 (2014) 145.
[23] H.-W. Park, J.-S. Park, J.H. Lee, K.-B. Chung, Electrochem. Solid-State Lett. 15 (2012) H133.
[24] T. Kamiya, K. Nomura, H. Hosono, J. Disp. Technol. 5 (2009) 273.
[25] B.K. Kim, J.S. Park, D.H. Kim, K.B. Chung, Appl. Phys. Lett. 104 (2014) 182106.